International Journal of Applied Mechanics
Vol. 7, No. 1 (2015) 1550009 (26 pages)

DOI: 10.1142/S1758825115400098

Imperial College Press
www.icpress.co.uk

Shape Optimization of Acoustic Enclosures Based on a Wavelet–Galerkin Formulation

S. Zhang and L. Cheng*

Department of Mechanical Engineering
The Hong Kong Polytechnic University, Hung Hom
Kowloon, Hong Kong SAR, P. R. China
**Li.cheng@polyu.edu.hk*

Received 26 May 2014
Revised 13 October 2014
Accepted 16 October 2014
Published 28 January 2015

The problem of the shape optimization of acoustic enclosures is investigated in this paper. A general procedure, comprising a Wavelet–Garlerkin formulation and a so-called vertex-driven shape optimization is proposed to deal with the general problem of internal sound field prediction and the optimization of the boundary shape. It is shown that, owing to the compactly supported orthogonal property and the remarkable fitting ability, Daubechies Wavelet can be used as a global basis to approximate the unknown sound field on a relatively large interval globally instead of piecewise approximation like most of element based methods do. This feature avoids meshing the boundary of the enclosure, although vertex points are needed to define the boundary shape, whose positions keep updating during the shape optimization process. A rectangular enclosure is used as benchmark to assess and validate the proposed formulation, by investigating the influence of some key parameters involved in the formulation. It was shown that the sound pressure along the entire boundary of the rectangular enclosure can be accurately approximated without meshing. The same enclosure with an inner rigid acoustic screen is then used to reduce the sound pressure level within a chosen area through optimizing the shape of the screen, which shows the remarkable potentials of the proposed approach as a shape optimal tool for inner sound field problems.

Keywords: Shape optimization; internal sound filed; irregular enclosure; wavelet-Galerkin.

1. Introduction

The acoustic problem inside an enclosure becomes increasingly important due to the extensive use of cavities in real life structures, such as industrial enclosures, office partitions, aircraft cabins and vehicle compartments [Liu *et al.*, 2006a] etc. Sound field inside a cavity depends on the cavity shape, which either impacts on the sound distribution in an acoustic system, or affects the coupling between the cavity and a surrounding flexible wall [Zheng and Wei, 2013; Geng and Li, 2012;

*Corresponding author.

Chen *et al.*, 2012] in a vibro-acoustic system [Fahy and Gardonio, 2007]. Typical examples include the shape optimization of the car body to improve the interior sound distribution in the acoustic design of automobile [Marburg and Hardtke, 2001; Koo *et al.*, 1998]; design of inner partitions in cavities [Succi, 1987]; optimization of internal partitions in mufflers [Lee and Kim, 2009; Chiu and Chang, 2008; Mimani and Munjal, 2011] or resonators [Kost *et al.*, 2011] etc. Therefore, topological or shape optimization of acoustic cavities is of significant relevance to both scientific research and engineering applications.

It is obvious that shape optimization of acoustic cavities requires a solver to calculate the internal sound field. Among existing methods, analytical solutions only apply to a few cavities with simple geometries such as rectangular or cylindrical, which allow separation of variables in Cartesian and cylindrical coordinate system, respectively [Levine, 2001]. For cavities of more complex shapes, various so-called semi-analytical methods were developed [Succi, 1987; Dowell *et al.*, 1977; Missaoui and Cheng, 1997], by pushing the analytical treatment to its limit before deploying numerical descretizations. Most of these methods, however, involve stringent limitation on the cavity shapes such as a slight distortion from a regular one [Succi, 1987], a combination of regular-shaped sub-cavities with known eigen-functions [Dowell *et al.*, 1977] or a combination of the aforementioned scenarios [Missaoui and Cheng, 1997; Anyunzoghe and Cheng, 2002]. As a last resort, numerical solvers such as finite element methods (FEM) and boundary element method (BEM) have long been recognized as the most versatile tools to deal with systems of various shapes. These numerical methods need to decentralize the model including building CAD model and meshing. In particular, if the enclosure shape is to be optimized to get a desired sound pressure distribution, the traditional FEM/BEM requires meshing the geometry in every optimization loop, which is time consuming and cumbersome. This seriously limits the FEM/BEM in the application of shape optimization [Liu *et al.*, 2006b]. Successful cases include local shape optimization [Marburg, 2002; Marburg and Hardtke, 2002] or local boundary modification [Givoli and Demchenko, 2000], in which only slight modification of the shape was entertained.

FEM/BEM discretizes the solution region into elements or short intervals, over which the solution is approximated using local basis such as polynomials of fixed order. For the local basis, continuity conditions must be imposed across sub-interval boundaries. This imposes tremendous difficulty in coping with boundary changes incurred in the shape optimization problems. This problem can be possibly solved if a global basis can be used. A global basis is the one in which the base functions have support over the entire region. However, conventional base functions such as polynomials and spline functions cannot provide a precise solution for the complex solution space like sound fields in the cavities [Peng and Cheng, 2008]. Lack of appropriate function basis becomes the bottleneck hampering the application of global expansion method in complex solution space. In a broader sense, there is a real need for developing flexible tools which are inductive to optimization of inner acoustics field.

The objective of this work is to explore the feasibility of using wavelets as global expansion functions under the Galerkin framework to solve the general cavity problem and its shape optimization in particular. For the sake of convenience, the method is referred to as wavelet-Galerkin Method (WGM), which largely inspires from the recent progress in using Wavelets for solving differential equations in various fields [Jaffard, 1992; Wang, 1998; Maleknejad and Lotfi, 2006]. Wavelet is shown to possess some appealing features such as compact support, flexible scaling and translation, and ability to express any square integrable function on the real axis. In the present work, Daubechies wavelet scaling function is used as basis function to expand the unknown sound pressure under Galerkin framework globally. This method will handle cavities of arbitrary shape without requiring any modal information *a priori*. Meanwhile the method does not need the meshing process like FEM/BEM does, owing to the extraordinary fitting ability of the Daubechies wavelet. A boundary treatment is then proposed, which is conducive to shape optimization in cavities.

In order to illustrate the process, we propose to investigate a general two-dimensional (2D) cavity formed by segments connected by a number of pre-set nodes. In a broad sense, the segments can be curves of any shapes such as arcs or spline, as long as they can be described by relatively simple curve functions. For illustration purposes, however, we will limit to straight segments. In this sense, only polygonal cavities will be dealt with in this paper. Without losing generality, different complex-shaped cavities can be approximated by moving the nodes. Figure 1 shows an example in which, by relocating the nodes, a general polygonal cavity can evolve to represent (a) a vehicle compartment, (b) an enclosure with partitions and (c) an aircraft cabin.

The outline of the paper is as follows. The proposed WGM is first formulated. Problems involved in the implementation phase including boundary treatment and the parameter selection of wavelets, such as the resolution level and the support length are investigated. A rectangular enclosure with exact solutions is selected as a

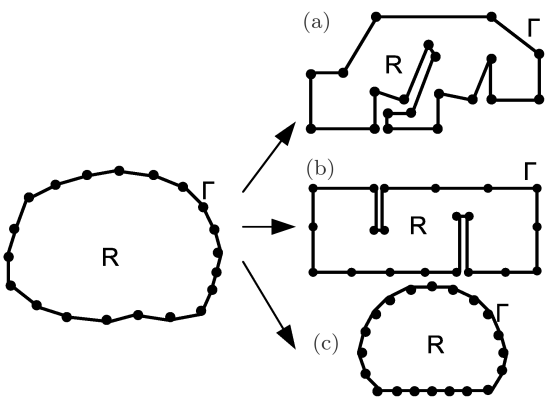

Fig. 1. Examples of a polygonal cavity and its evolution.

benchmark for validation purposes. Applications to a rectangular enclosure with an inner partition are demonstrated for further validation. The same example is then used to optimize the partition shape toward the creation of a quiet zone inside the enclosure.

2. Formulation

2.1. *Kirchhoff–Helmholtz equation and Galerkin framework*

Consider a general acoustic area R enclosed by a boundary Γ as shown in left part of Fig. 1. The wave equation governing the sound pressure field excited by a harmonic source in the enclosure reads

$$\nabla^2 p + k^2 p = -i\omega\rho_0 Q\delta(\mathbf{r} - \mathbf{r_s}), \tag{1}$$

where p is the acoustic pressure; $k = \omega/c - i\alpha$ with ω, c ρ_0 and α being the angular frequency of the excitation source, the sound speed, density and the absorption coefficient of the acoustic medium, respectively. $i = \sqrt{-1}$; Q is the source strength; and $\delta(\mathbf{r} - \mathbf{r_s})$ is Dirac delta function.

The sound field inside the enclosure can be described by Kirchhoff–Helmholtz equation which is the boundary integral form of Eq. (1) [Bai, 1992]:

$$\beta(\mathbf{r_0})p(\mathbf{r_0}) + \int_\Gamma p(\mathbf{r})\frac{\partial G}{\partial n}(\mathbf{r}, \mathbf{r_0})\mathrm{d}\Gamma - \int_\Gamma G(\mathbf{r}, \mathbf{r_0})\frac{\partial p}{\partial n}(\mathbf{r})\mathrm{d}\Gamma + i\omega\rho_0 QG(\mathbf{r_s}, \mathbf{r_0}) = 0, \tag{2}$$

where

$$\beta(\mathbf{r_0}) = \begin{cases} 0 & \text{if } \mathbf{r_0} \notin R \cup \Gamma \\ 1 & \text{if } \mathbf{r_0} \in R \\ 1/2 & \text{if } \mathbf{r_0} \in \Gamma, \Gamma \text{ a smooth surface} \\ \theta/4\pi & \text{if } \mathbf{r_0} \in \Gamma, \Gamma \text{ a nonsmooth surface} \end{cases}.$$

The complex variable $p(\mathbf{r})$ denotes the sound pressure at the location $\mathbf{r}$. The position vector $\mathbf{r_0}$, $\mathbf{r}$ and $\mathbf{r_s}$ denote the positions of the calculated point where the pressure is being evaluated, the position of a point on the surface S and the position of any sources inside the enclosure. The free-space Green's function is $G(\mathbf{r}, \mathbf{r_0}) = -iH_0^{(2)}(kr)/4$ for the Helmholtz equation in a 2D space. $r = |\mathbf{r_0} - \mathbf{r}|$. The directional directive $\partial/\partial n \equiv \mathbf{n} \cdot \nabla$ with $\mathbf{n}$ being the outward normal to the boundary Γ.

The Kirchhoff–Helmholtz equation shows that the acoustic pressure inside the enclosure can be determined by the normal particle velocity and the pressure at the boundary, as well as the inner sources. The pressure and the velocity at the boundary, however, are inter-related. When $\mathbf{r_0}$ and $\mathbf{r}$ are all chosen at the boundary, the pressure at the boundary can be worked out. Then the solutions at the boundary are used in Eq. (2) again to get the inner sound pressure, leading to the boundary integral equation form.

If the boundary is meshed to short interval and polynomials or other relative simple functions are used to expand the unknown field in the short interval at the boundary, the approach retreats to classical BEM. In contrast to BEM, the Galerkin approach does not require that the boundary integral equations be satisfied at every single point. Instead, Eq. (2) is enforced in a weighted average as:

$$\int_{\Gamma_\tau} \hat{p}(\tau)\beta(\tau)p(\tau)\mathrm{d}\Gamma_\tau + \int_{\Gamma_\tau} \hat{p}(\tau) \int_{\Gamma_\sigma} p(\sigma)\frac{\partial G(\sigma,\tau)}{\partial n}\mathrm{d}\Gamma_\sigma \mathrm{d}\Gamma_\tau$$
$$- \int_{\Gamma_\tau} \hat{p}(\tau) \int_{\Gamma_\sigma} G(\sigma,\tau)\frac{\partial p(\sigma)}{\partial n}\mathrm{d}\Gamma_\sigma \mathrm{d}\Gamma_\tau + \int_{\Gamma_\tau} \hat{p}(\tau)Q\delta(\mathbf{r}-\mathbf{r_s})G(\sigma,\tau)\mathrm{d}\Gamma_\sigma \mathrm{d}\Gamma_\tau = 0, \tag{3}$$

where τ and σ are points at the boundary; $\alpha(\tau)$ is defined by Eq. (2); $\hat{p}(\tau)$ is a weighting function. This formulation carries a clear interpretation: the approximate Galerkin solution is the exact solution projected onto the subspace consisting of all functions which are linear combinations of the shape functions. The Galerkin solution is therefore the linear combination which is the "closest" to the exact solution.

To solve Eq. (2), the unknown function $p(\sigma)$ and $\frac{\partial p(\sigma)}{\partial n}$ can be expanded as

$$p(\sigma) = \sum_i a_i \varphi_i(\sigma), \tag{4}$$

$$\frac{\partial p(\sigma)}{\partial n} = \sum_j b_j \varphi_j(\sigma). \tag{5}$$

According to Galerkin framework, the weighting function $\hat{p}(\tau)$ can be set as

$$\hat{p}(\tau) = \varphi_k(\tau), \tag{6}$$

where $\varphi_i(\sigma)$, $\varphi_j(\sigma)$ and $\varphi_k(\tau)$ are expansion set, which can be any function, such as polynomials. Wavelets will be adopted here. The difference between these two bases will be compared in Sec. 3.1.3. a_i and b_j are unknown coefficients.

After substituting Eqs. (4)–(6) into Eq. (3), Eq. (3) can be rearranged into the following matrix form

$$\mathbf{La} + \mathbf{Mb} = \mathbf{R}, \tag{7}$$

where

$$\mathbf{L}_{k,i} = \int_{\Gamma_\tau} \beta(\tau)\varphi_k(\tau)\varphi_i(\tau)d\Gamma_\tau + \int_{\Gamma_\tau} \varphi_k(\tau) \int_{\Gamma_\sigma} \varphi_i(\sigma)\frac{\partial G(\sigma,\tau)}{\partial n}d\Gamma_\sigma d\Gamma_\tau, \tag{8}$$

$$\mathbf{M}_{k,j} = -\int_{\Gamma_\tau} \varphi_k(\tau) \int_{\Gamma_\sigma} \varphi_j(\sigma)G(\sigma,\tau)d\Gamma_\sigma d\Gamma_\tau, \tag{9}$$

$$\mathbf{R}_k = -\int_{\Gamma_\tau} \varphi_k(\tau) \int_{\Gamma_\sigma} q(\mathbf{r_s})G(\sigma,\tau)d\Gamma_\sigma d\Gamma_\tau, \tag{10}$$

$$\mathbf{a}_i = a_i, \tag{11}$$

$$\mathbf{b}_j = b_j, \tag{12}$$

in which $\mathbf{a}$, $\mathbf{b}$ are unknown coefficient vectors for acoustical pressure p and derivative of acoustical pressure $\partial p(\sigma)/\partial n$, respectively. Equation (7) applies to the boundary. For conventional Dirichlet or Neumann boundary conditions, $\mathbf{a}$ or $\mathbf{b}$ vanishes; for mixed boundary condition, a relationship between $\mathbf{a}$ and $\mathbf{b}$ exists. For multiple boundary conditions, the solution can be worked in the corresponding boundary segments.

2.2. *Wavelet basis and global expansion*

The prevailing idea of the proposed wavelet-Garlerkin formulation is to approximate the unknown sound field at the *entire* boundary by a combination of predefined wavelet bases, as expressed in Eqs. (4) and (5). This is fundamentally different from BEM, or other element based method, in which the boundary is meshed into small pieces to be approximated locally. The obvious challenge is to find a suitable basis with necessary fitting capability to approximate the solution on a relatively large interval globally instead of approximating a function piecewise. The apparent benefit is that, without meshing the boundary, the method can be very efficient especially for shape optimization problems. Hereafter, we will demonstrate that wavelet functions can fulfill this requirement.

2.2.1. *Daubechies wavelet*

Daubechies wavelet is a family of compactly supported orthogonal wavelets including both highly localized and highly smooth members. Each wavelet member is governed by a set of L (an even integer) coefficients $\{h_j : j = 0, 1, \ldots, L-1\}$ through two-scale relations

$$\varphi(x) = \sum_{j=0}^{L-1} h_j \varphi(2x - j) \tag{13}$$

and

$$\psi(x) = \sum_{j=2-L}^{1} (-1)^j h_{1-j} \varphi(2x - j), \tag{14}$$

where $\varphi(x)$ and $\psi(x)$ are called scaling function and mother wavelet, respectively. The fundamental support of the scaling function $\varphi(x)$ is the interval $[0, L-1]$ while that of the corresponding wavelet $\psi(x)$ is in the interval $[1 - L/2, L/2]$. The coefficients h_j in the two-scale relation (13) are called the wavelet filter coefficients. Values of these coefficients can be found in the literature [Chen *et al.* 2006].

Correspondingly, the scaling function $\varphi(x)$ has the following properties:

$$\int_{-\infty}^{\infty} x^k \psi(x) \mathrm{d}x = 0, k = 0, 1, \ldots, L/2 - 1. \tag{15}$$

It is noted that the property (15) is equivalent to that of the elements of the set $\{1, x, \ldots, x^{L/2-1}\}$ are linear combinations of $\varphi(x-k)$, integer translates of $\varphi(x)$. So the scaling function $\varphi(x)$ can be used to approximate a function on an interval [Chen *et al.*, 2006].

2.2.2. *Wavelet expansion and basis selection*

Choosing Daubechies wavelet as basis, Eqs. (4)–(6) can be converted to

$$p(\sigma) = \sum_j a_{m,j} \varphi_{m,j}(\sigma), \tag{16}$$

$$\frac{\partial p(\sigma)}{\partial n} = \sum_j b_{m,j} \varphi_{m,j}(\sigma), \tag{17}$$

$$\hat{p}(\tau) = \varphi_{m,j'}(\tau), \tag{18}$$

$$\varphi_{m,j}(x) = 2^{m/2} \varphi(2^m x - j), \tag{19}$$

where $\varphi(\cdot)$ is the wavelet scaling function; m the resolution level; j an integer translation and L_r the expansion length. A single resolution Daubechies wavelet scaling function ($j = 0$) and its series with different translations ($j = -3, -2, \ldots 4, 5$) are shown in Fig. 2. It shows that wavelet scale functions have compact support, flexible scaling, translation and strong oscillation. These properties provide great potential in global expansion, especially for problems with complex boundary.

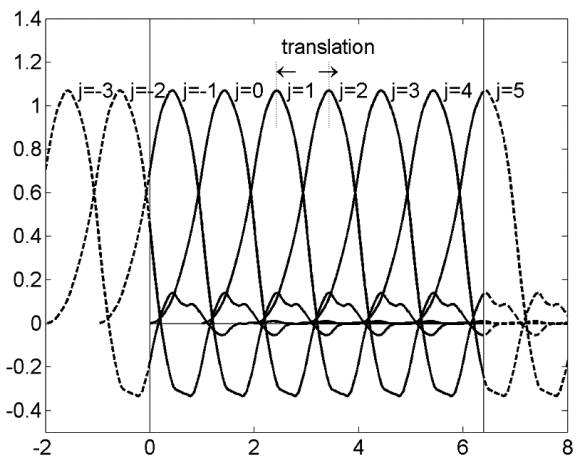

Fig. 2. Single resolution Daubechies wavelet scaling functions series with different translations.

The problem now is to choose the suitable range of integer translation j. Considering Eq. (16), all the wavelet scaling functions between the expansion domain $[0, L_r]$ should be included into the expansion set. However, using Eqs. (16) and (17) in Eq. (7) requires the calculation of $\int_{\Gamma_\tau} \varphi_k(\tau) d\Gamma_\tau$. As the wavelet scale function $\varphi_k(\tau)$ is a compact support function, when $\int_{\Gamma_\tau} \varphi_k(\tau) d\Gamma_\tau$ equals to zero, the matrix system $\mathbf{L}$, $\mathbf{M}$ and $\mathbf{R}$ defined by Eqs. (8), (9) and (10) are singular and the problem becomes underdetermined. So the expansion set of Eqs. (16) and (17) should be modified as below to avoid such occurrence:

$$p(\sigma) = \sum_{j=-L+2+l_1}^{2^m \lceil L_r \rceil - 1 - l_2} a_{m,j} \varphi_{m,j}(\sigma), \tag{20}$$

$$\frac{\partial p(\sigma)}{\partial n} = \sum_{j=-L+2+l_1}^{2^m L_r - 1 - l_2} b_{m,j} \varphi_{m,j}(\sigma), \tag{21}$$

where $l_1 > 0$ and $l_2 > 0$ are correction values. Procedure to determine l_1 and l_2 are detailed as follows. $\lceil \bullet \rceil$ means rounding the number to the nearest integers greater than or equal to itself.

The integration of wavelet scale function can be defined as

$$\theta(x) = \int_0^x \varphi(y) dy. \tag{22}$$

Method for calculating the above integration is given by Chen *et al.* [1996]. In light of the above definition, $\int_{\Gamma_\tau} \varphi_k(\tau) d\Gamma_\tau$ can be converted to

$$\int_0^{L_r} \varphi_{m,j}(x) \mathrm{d}x = 2^{-m/2} (\theta(2^m L_r - j) - \theta(-j)), \tag{23}$$

where $j = -L + 2 + l_1, \ldots, 2^m \lceil L_r \rceil - 1 - l_2$. j is substituted into Eq. (23) and the correction values can be worked out considering the property of $\theta(x)$ [Chen *et al.*, 1996] to avoid zero value. This gives

$$l_1 = 0, \tag{24}$$

$$l_2 = \lfloor (2^m \lceil L_r \rceil - L_r) \rfloor. \tag{25}$$

Equations (20) and (21) can then be converted to

$$p(\sigma) = \sum_{j=-L+2}^{2^m \lceil L_r \rceil - 1 - \lfloor (2^m \lceil L_r \rceil - L_r) \rfloor} a_{m,j} \varphi_{m,j}(\sigma), \tag{26}$$

$$\frac{\partial p(\sigma)}{\partial n} = \sum_{j=-L+2}^{2^m \lceil L_r \rceil - 1 - \lfloor (2^m \lceil L_r \rceil - L_r) \rfloor} b_{m,j} \varphi_{m,j}(\sigma). \tag{27}$$

The above modified expansion set will guarantee nonzero values for $\int_{\Gamma_\tau} \varphi_k(\tau) \mathrm{d}\Gamma_\tau$ such that avoiding the singularity of $\mathbf{L}$, $\mathbf{M}$ and $\mathbf{R}$. $\lfloor \bullet \rfloor$ means rounding the number to the nearest integers less than or equal to itself.

As an example, Fig. 2 shows how to choose the expansion set. The wavelet scale functions with zero value in the expansion domain or with the value that can lead to the zero integration value of $\int_{\Gamma_\tau} \varphi_k(\tau) d\Gamma_\tau$ should be removed from the expansion set (dashed line).

2.3. *Shape optimization*

The proposed WGM is a global expansion method in the sense that fine meshing of the geometry model is not needed. Taking advantage of this feature, a shape optimization strategy is proposed as follows.

A procedure named vertex-driven shape optimization is demonstrated in Fig. 3 in which the boundary of a polygonal cavity to be optimized is defined by a number of nodal points/nodes. Some of the nodal points have fixed positions, referred to as fixed points, whilst others are called control points whose positions can be changed to form a boundary of different shape. Upon assigning initial positions to all nodal points, WGM approach is deployed to calculate the inner sound field to get the cost function determined by the optimization objective. During the optimization, the positions of the control points will be adjusted to get an optimized result. In the whole procedure, there is no need to mesh between the points, the positions of the control points and the shape of the cavity will not stop changing until convergence to the final optimal shape is achieved.

In principle, there are various physical quantities to be optimized. As an example, the problem of optimizing the shape of an acoustic enclosure to control the sound pressure level, L, in a predefined local area inside the enclosure is chosen. L is

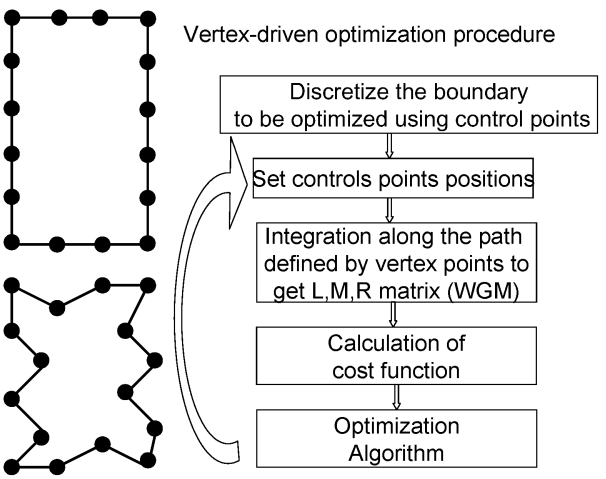

Fig. 3. Vertex-driven optimization procedure.

approximated as

$$\min_{\mathbf{r}\in R} L(\mathbf{r}) = 10\log\frac{1}{n}\sum_{i=1}^{n} 10^{L_i(\mathbf{r})/10}\text{dB}, \tag{28}$$

where $L_i(\mathbf{r})$ is the SPL of the test point i at location $\mathbf{r}$. $R = \{\mathbf{r}\,|\,\mathbf{r} \in S\}, S$ is the pre-defined quiet-area in the cavity.

In principle, any optimization algorithm can be used. Considering the complicity of the objective function with unknown knowledge on its derivatives, an optimization algorithm based on genetic algorithm (GA) [Renner and Ekárt, 2003] will be adopted here. Global optimization methods like GAs show robust behavior, especially if the design analysis algorithm has convergence problems and does not return with objective function values for all demanded design points. MIGA is a class of general-purpose search method providing a remarkable balance between exploration and exploitation of the results that is characteristics of GA. The main feature of MIGA that distinguishes it from the traditional GA is the fact that each population of individuals (i.e., a set of probable solutions) is divided into several sub-populations called "Island". All traditional genetic operations, such as selection, crossover and mutation, are performed separately on each Island. Some individuals are then selected from each Island and are migrated to different Islands periodically. Two parameters control the migration process: migration interval and migration rate. The migration operation in MIGA keeps the diversity of probable solutions and hence increases the chance of obtaining the global optimal solution. Discussion on the optimization algorithm itself is beyond the scope of this paper.

Making use of commercial optimization package iSight in conjunction with the Matlab code for the WGM solver, the shape optimization procedure is implemented as shown in Fig. 4. The program iSight is used to define the optimization flow consisting of initialization, an optimization loop and post-processing. The optimization routine based on MIGA supplied by iSight interacts with the acoustic solver based on WGM. When the optimization program requires a new design evaluation, iSight invokes a Matlab script which calculates the acoustic response with a new updated shape, which is feedbacked to MIGA optimizer. The optimization loop proceeds as the enclosure shape evolves until the optimized shape is reached. Due to the parallel property of MIGA, the optimization controlled by iSight may be split into multiple programs running in a heterogeneous computational environment.

3. Numerical Studies

3.1. *Numerical examples*

The WGM was first applied to a 2D rectangular enclosure for validation purposes. The enclosure has a dimension of 2.0 m by 1.2 m. A monopole source is placed inside the rigid-walled enclosure (0.1 m, 0.1 m) as shown in Fig. 5. The original point is set at left bottom.

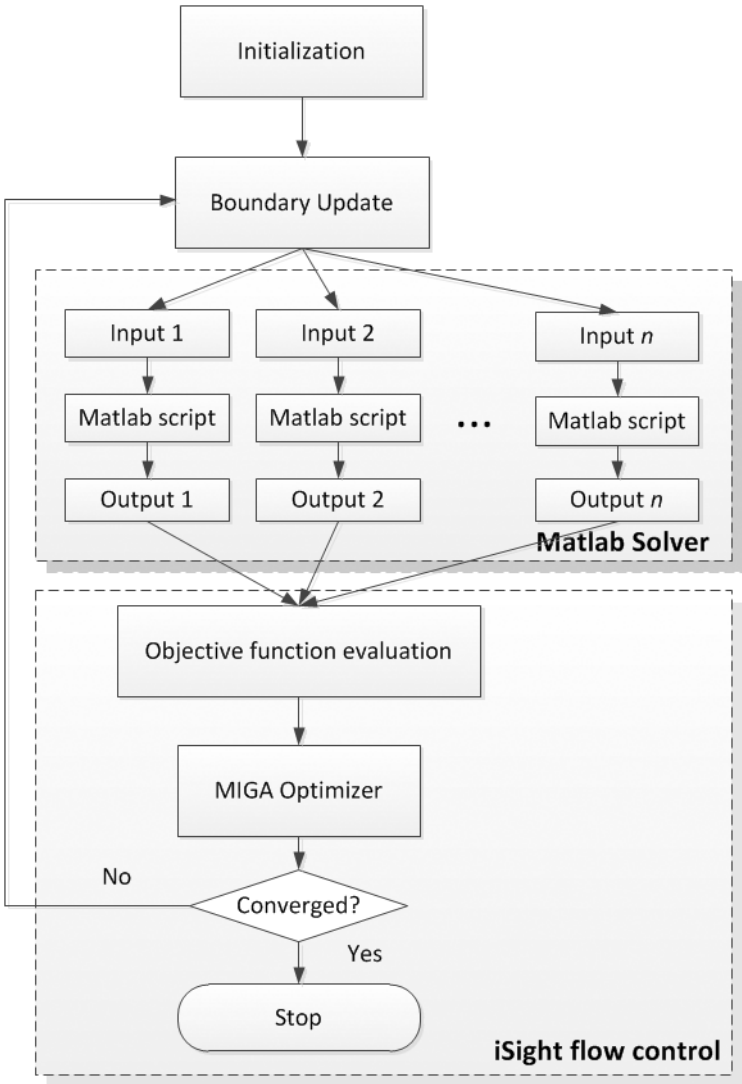

Fig. 4. Sketch of the shape optimization procedure realized with iSight.

3.1.1. *Validation*

The frequency response of the sound pressure at (1.9 m, 0.1 m) was compared with analytical solutions based on modal superposition using 2500 modes [Anyunzoghe and Cheng, 2002] in Fig. 6. In the calculation, the absorption coefficient α was set to be 0.01. WGM used $L = 10$ and $m = 5$ wavelet basis. Figure 6 shows a perfect agreement between the two methods since the two lines are barely distinguishable. The pressure contours in the cavity, as well as the error in terms of

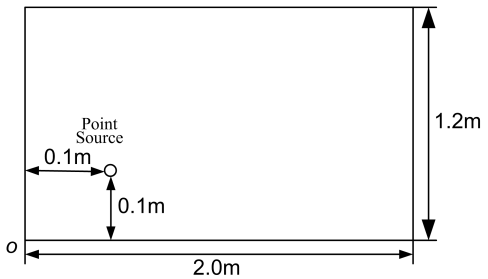

Fig. 5. Rectangular enclosure with/without internal partial partition.

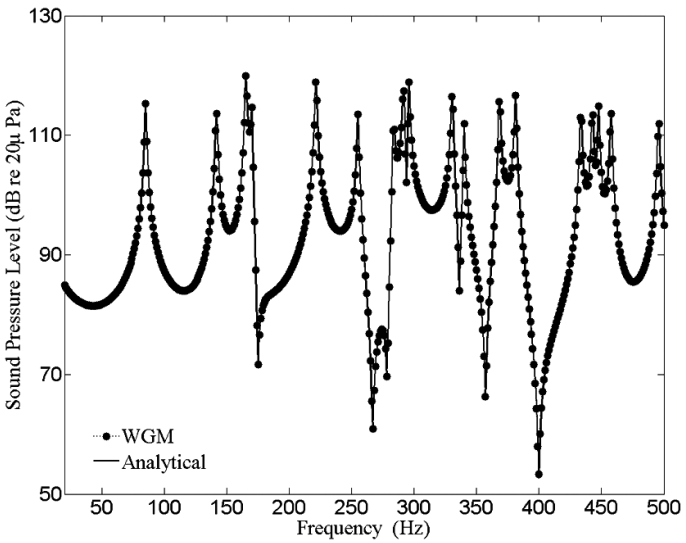

Fig. 6. Magnitude of the sound pressure at the receiver in the rectangular enclosure using WGM and analytical modal superposition method. The sound source is located at (0.1 m, 0.1 m).

sound pressure level, at one arbitrary frequency of 115 Hz are also compared in Fig. 7. Again, the pressure responses are almost the same everywhere inside the cavity. The maximum deviation is typically below 0.5 dB as shown in Fig. 7(c). Same comparisons carried out for other frequencies (not shown here) also show a good agreement between the two sets of results. It is relevant to note that in the WGM, no meshing was performed and entire boundary, comprising four edges, was treated as one single piece, over which the sound pressure was approximated using the same set of wavelet approximation.

3.1.2. *Convergence and adaptive rule*

Using the same configuration, the convergence of WGM and adaptive rule are investigated. The error with respect to the exact solution is calculated considering

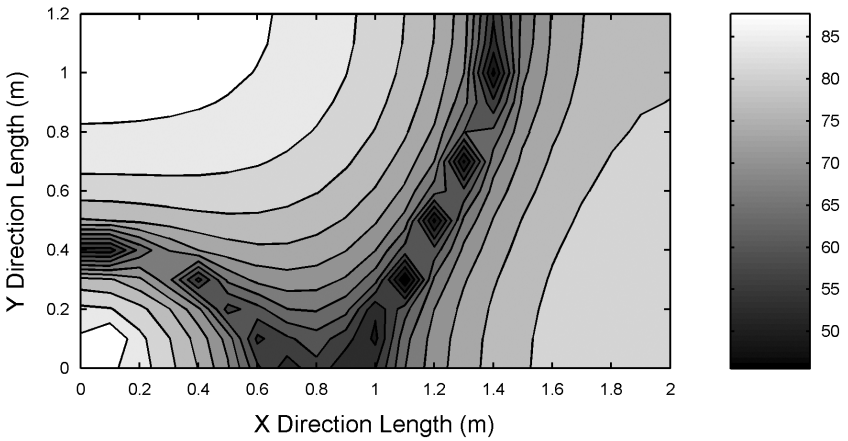

(a)

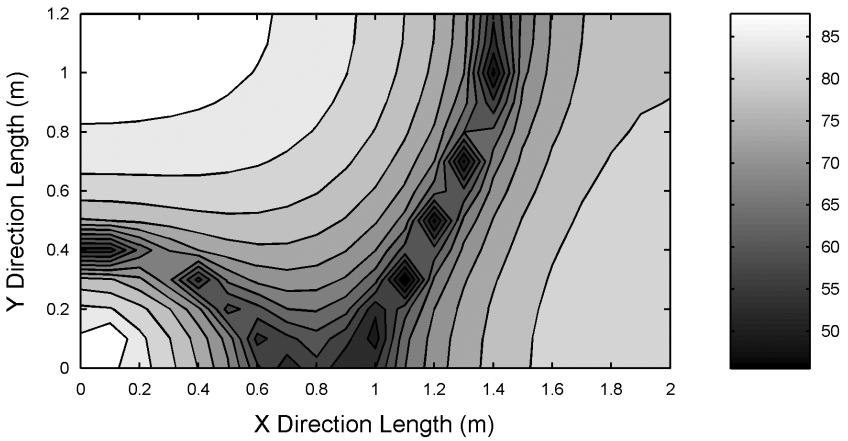

(b)

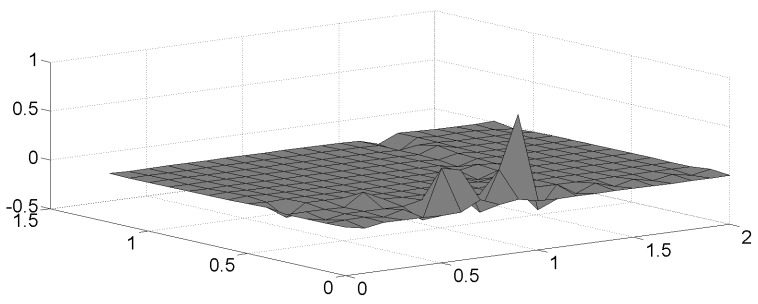

(c)

Fig. 7. Contour plots showing the pressure field at 115 Hz inside the rectangular enclosure. The contour lines are at 5 dB intervals. (a) WGM, (b) modal superposition, (c) error in the sound pressure level field at 115 Hz between WGM and modal superposition method.

different wavelet support lengths L, wavelet resolution m and Gauss integration point number.

Figure 8 shows the absolute error of the frequency response function between the source and the receiver calculated by WGM compared with the modal superposition model from 20 Hz to 500 Hz. Figures 8(a) and 8(b) set the wavelet resolution m fixed and consider different wavelet support lengths L. When $m = 1$, the absolute error becomes extremely large as the frequency is over 250 Hz (Fig. 8(a)). When $m = 3$, Fig. 8(b) shows that the absolute error is quite small compared with $m = 1$. In both cases, the error varies slightly with L. These observations seem to suggest that the

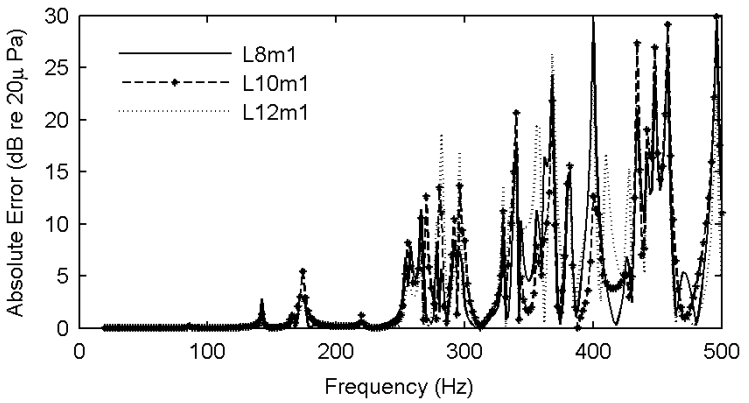

(a)

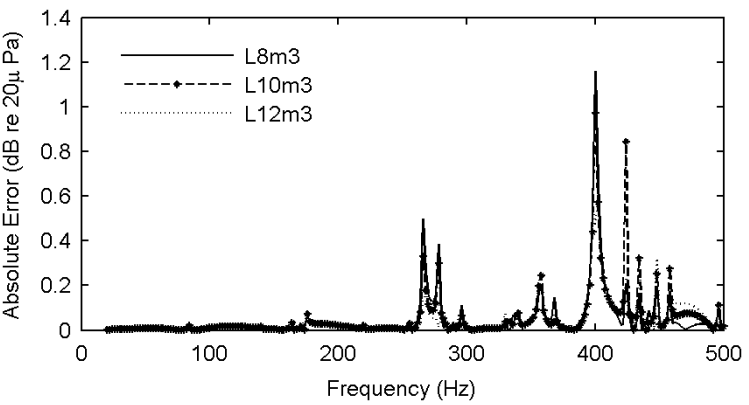

(b)

Fig. 8. (a) Absolute error at the receiver point using different wavelet support lengths $L = 8$ (solid), $L = 10$ (dashed) and $L = 12$ (dotted) with wavelet resolution m being fixed at 1. (b) Absolute error at the receiver point using different wavelet support lengths $L = 8$ (solid), $L = 10$ (dashed) and $L = 12$ (dotted) with wavelet resolution m being fixed at 3. (c) Absolute error at the receiver point using different wavelet resolution $m = 2$ (solid), $m = 3$ (dashed) and $m = 4$ (dotted) with wavelet support length L being fixed at 8.

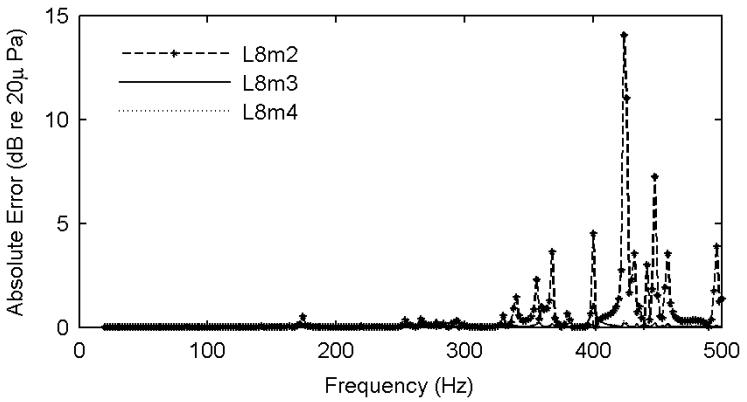

(c)

Fig. 8. (*Continued*)

wavelet resolution m significantly impacts on the calculation accuracy, while the wavelet support length L only exerts slight influences.

For a given support length L, more accurate result can be obtained as the wavelet resolution level m increases up to 4. This can be better shown in Fig. 8(c) with $L = 8$. However, there seems to have an optimal point starting from which error starts to increase when further increasing m. Considering Eq. (2), the interior sound field is determined by the sound pressure at the boundary. So the maximum error at the boundary with respect to the analytical result is chosen as criteria during the simulation.

$$E = 20\log(\max(p_\Gamma - p_{\Gamma_a})/p_{\text{ref}}), \tag{1}$$

where p_{Γ_a} is the sound pressure calculated by analytical method, $p_{\text{ref}} = 20\,\mu\text{Pa}$. Figure 9(a) shows the maximum error E at the boundary defined by Eq. (1) at 480 Hz. The error first decreases and then increases while m increases starting from $m = 4$. In order to explain this phenomenon, Fig. 9(b) shows the magnitude of the singular values of the matrix $\mathbf{L}$ when m varies from 4 to 7. It can be seen that the singular values fall off at a relatively constant rate until around the 280th singular value where the level begins to decay rapidly. The implication is that with this number of Gauss integration point the use of more than 280 wavelet bases is likely to produce a poorly conditioned result. Small singular values imply that the wavelet bases have almost no effect on the pressure component that corresponds to that singular value. The number of Gauss integration point for all the cases above is set as 340.

The problem becomes better conditioned by increasing the number of Gauss integration point. This can be illustrated by looking at the singular values of the matrix $\mathbf{L}$ with the support length $L = 8$ and resolution $m = 6$ at 480 Hz (Fig. 10). In this case the smallest singular value using 682 Gauss integration point is more

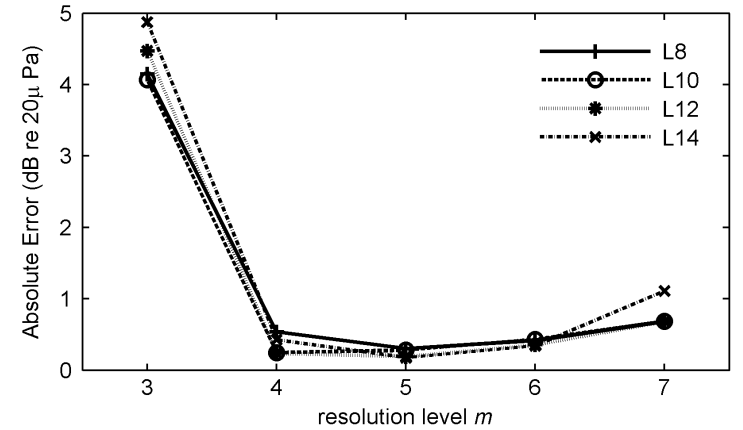

(a)

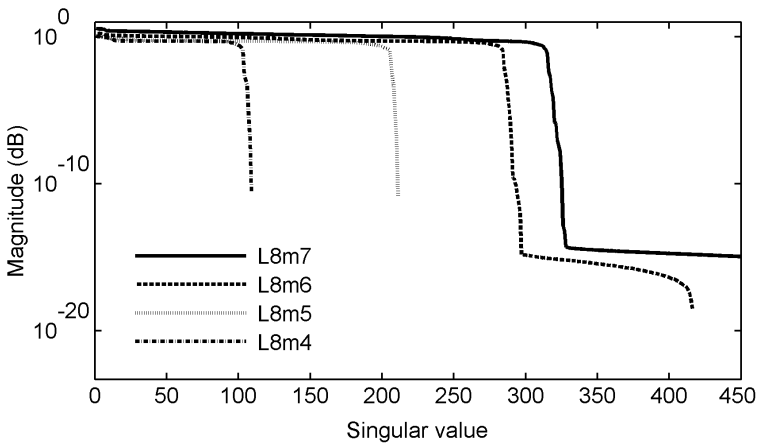

(b)

Fig. 9. (a) Maximum absolute error at the boundary using different wavelet support lengths $L = 8(+)$, $L = 10(\mathrm{o})$, $L = 12(*)$ and $L = 14(\mathrm{x})$ while wavelet resolution m is increased from 3 to 7 at 480 Hz. (b) Magnitude of the singular values of the matrix L, using different wavelet resolution $m = 4$ (dash dot), $m = 5$ (dotted), $m = 6$ (dashed), and $m = 7$ (solid) while wavelet support length $L = 8$ at 480 Hz.

than 7 orders of magnitude larger than that using 340 Gauss integration point. Consequently, the error decreases by using more Gauss points (Fig. 10). However, an increase in the number of Gauss points will not take effect for low wavelet resolution level, as illustrated in Fig. 10 with $m = 4$, in which case the singular value remains the same when number of Gauss points increases. One plausible reason is that for lower wavelet resolution level, fewer Gauss points is enough for evaluation, similar to sampling points used in signal processing. But for higher wavelet resolution level, more Gauss integration points are needed. If the level of error is unacceptable,

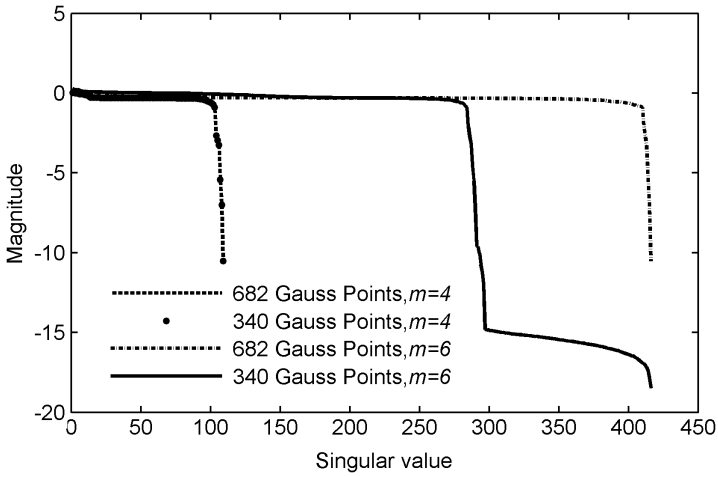

Fig. 10. Magnitude of the singular values of the matrix L using 682 Gauss integration points with resolution $m = 4$ (dotted), 340 Gauss integration points with resolution $m = 4$ (▪), 682 Gauss integration points with resolution $m = 6$ (dash dot) and 340 Gauss integration points with resolution $m = 6$ (solid) at 480 Hz.

potentially both the resolution level and the Gauss integral number need to be increased. Based on the above, the following adaptive algorithm is proposed:

Step 1. Set an acceptable threshold for the error at boundary defined by Eq. (29);

Step 2. Set an initial wavelet resolution level m and the Gauss integration point number. For each frequency, calculate the maximum error at the boundary. If the maximum error is larger than threshold preselected go to Step 3, otherwise continue the calculation.

Step 3. Increase the wavelet resolution level m if the maximum error is decreased while m is increased until the threshold is met. Otherwise, the Gauss integration point number should be increased to meet the threshold. Set the new wavelet resolution level m and the Gauss integration point number as default, and go to Step 2.

3.1.3. *Comparisons with polynomial basis*

The exceptional fitting capability of the wavelet basis in the proposed WGM scheme to approximate the solution on a relatively large interval globally is demonstrated in this section. This has been done by making comparisons with polynomial basis using the previous rectangular cavity. For a fair comparison, high order linear polynomials are deployed. The sound source excitation is deliberately put close to the boundary at (1.1 m, 0.1 m), in order to better show the phenomenon.

Figure 11 compares the magnitude of frequency response at the receiver obtained in the following three scenarios: using 58 wavelet basis (▪) with $L = 10$ and $m = 3$; using 180 polynomial terms (dashed) and modal superposition using 2500 modes

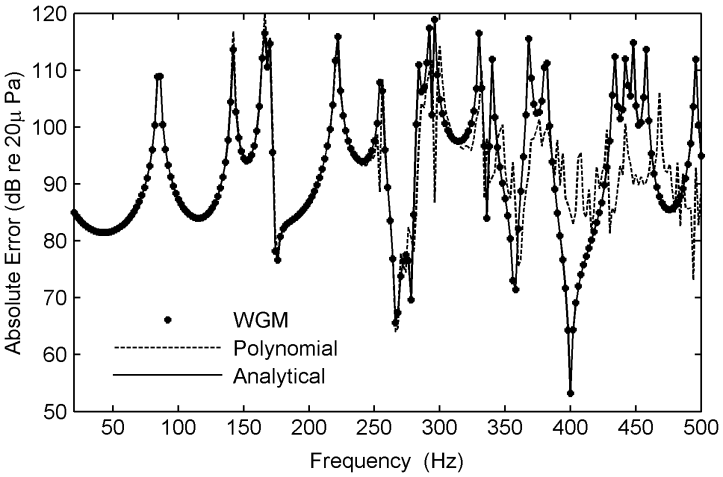

Fig. 11. Magnitude of the sound pressure at the receiver in the rectangular enclosure using 58 wavelet basis (*), 180 polynomial basis (dashed) and modal decomposition (solid).

(solid) from 20 Hz to 500 Hz. It can be seen that the responses calculated using wavelet basis and modal method match quite well. However, as the frequency increases, the result of polynomial basis deviates from the result of analytical solution more and more. This can be interpreted as a result of the difference in the fitting ability between the polynomial basis and wavelet basis. As the frequency increases, the sound field in the cavity becomes more complex, and much more polynomial terms are needed to achieve acceptable global expansion.

To further support the aforementioned argument, Fig. 12 shows the magnitude of the frequency response along the entire boundary of the rectangular enclosure at 80 Hz. It can be seen that WGM gives a perfect description of the sound pressure variation over the entire boundary as compared to the analytical solutions, whilst the error due to the polynomial basis can be clearly seen, especially near the sound source position, where the sound distribution is more complex due to its proximity to the sound source. It is obvious that wavelet basis shows its strong ability to carry out global expansion versus polynomial basis. The fundamental reason behind this can be analyzed by comparing the magnitude of the singular values for the two bases. It can be observed that the singular values of wavelet basis is kept at almost the same level while those of polynomial basis fall off at a relatively large rate, reaching the ill-condition scenario much easier than wavelet basis does.

Similar analysis was conducted for a higher frequency at 280 Hz. For comparison purposes, results using 111 wavelet basis with $L = 10$ and $m = 4$, and 180 polynomial basis are compared against analytical modal solutions using 2500 modes. Figure 13 shows that, along the boundary of the enclosure, the accuracy of the polynomial basis degrades seriously while wavelet basis still maintains its high accuracy.

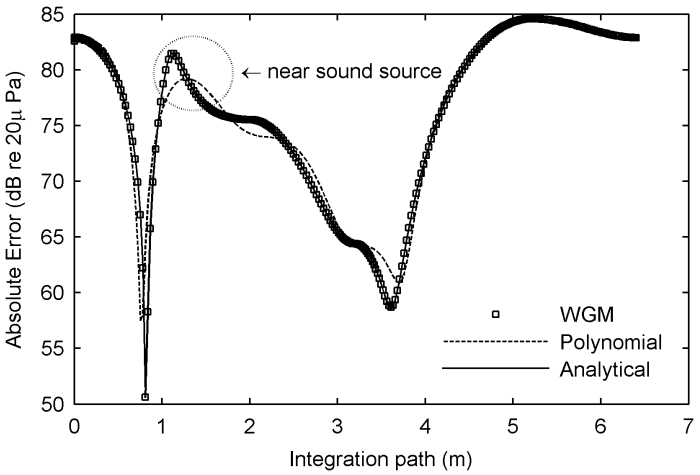

Fig. 12. Magnitude of the sound pressure along the boundary in the rectangular enclosure using 58 wavelet basis (□) with $L = 10$ and $m = 3$, 180 polynomial basis (dashed) and modal decomposition (solid) at 80 Hz.

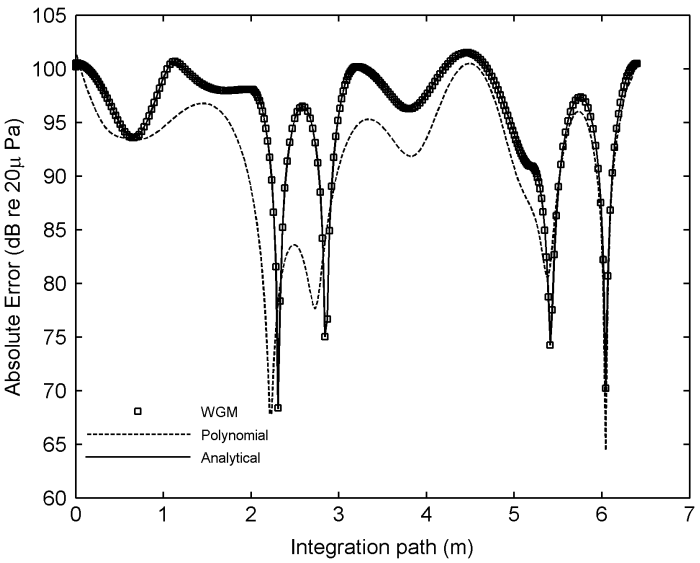

Fig. 13. Magnitude of the sound pressure along the boundary in the rectangular enclosure using 111 wavelet basis (□) with $L = 10$ and $m = 4$, 180 polynomial basis (dashed) and modal decomposition (solid) at 280 Hz.

Based on the above analysis, two important points are worth noting. Firstly, the wavelet basis shows high performance at global expansion under the Galerkin framework, even when handling complex sound field. Secondly, compared with the traditional polynomial basis, the wavelet basis is more robust against ill-condition problem.

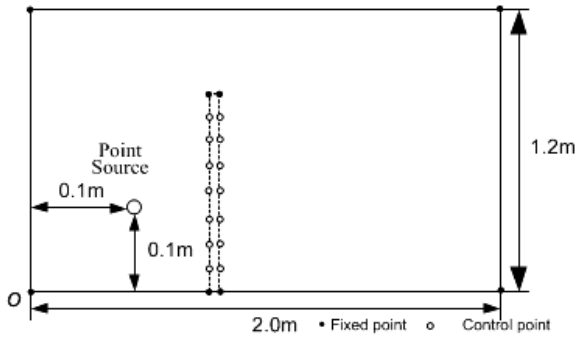

Fig. 14. A rectangular enclosure with an internal partial partition.

3.2. *Rectangular cavity with an internal partial partition*

WGM is used to handle a rectangular cavity with an internal partial partition, as depicted in Fig. 14. The rectangular cavity has the same dimension as the one used previously, with an acoustically rigid internal wall of thickness 0.002 m located at (0.8 m, 0.0 m).

3.2.1. *Validation*

Before optimization, the result obtained from the WGM is first compared with the FEM solutions from SYSNOISE for validating the implementation of the WGM. In the WGM, $L = 10$, $m = 3$. Figure 15 shows that the results obtained using these

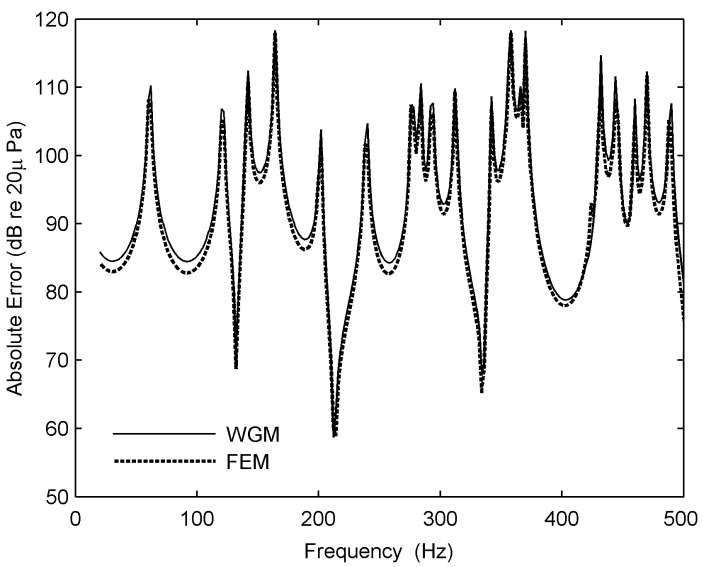

Fig. 15. Magnitude of the sound pressure at the receiver in the rectangular enclosure with an internal partial partition using wavelet basis (solid) and FEM by SYSNOISE (dashed).

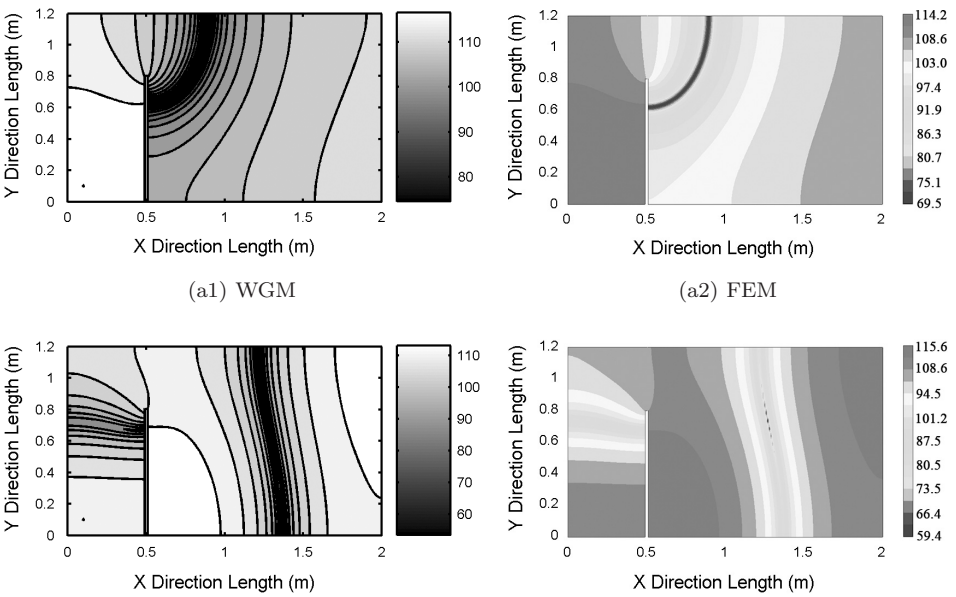

Fig. 16. Contour plots showing the sound pressure distribution inside the rectangular enclosure with an internal partial partition for the first two modes. Results were obtained using WGM (left column) and SYSNOISE right column), respectively. The contour lines are at 5 dB intervals. (a1, a2): First mode at 62 Hz; (b1, b2) second mode at 121 Hz.

two methods match well and the maximum error over the whole frequency range is about 1 dB. This comparison is supplemented with pressure contours in the cavity at the first two modes in Fig. 16. The sound pressure distribution is found to be almost the same everywhere inside the cavity between the two sets of results. This simulation confirms that the WGM can be used to accurately model the acoustic field inside a cavity when complexities are present inside.

3.2.2. *Optimization of the internal partition for the creation of a quiet zone*

As an example, the shape optimization procedure, as detailed in Sec. 2.3, is applied to the above configuration to show the capability of the proposed WGM in shape optimization problem. As optimization objective, the sound pressure level within the rectangular box behind the partition (Fig. 16(a)) is to be minimized at 121 Hz by changing the shape of the partition, as defined by Eq. (28). The rectangular box is 0.3 m by 0.4 m with its left bottom corner located at (0.8 m, 0.3 m). 44 positions, uniformly distributed inside the box, have been used to calculate the average SPL. The distance between each test point is 0.01 m.

As illustrated in Fig. 14, the boundary of the cavity, as well as the bottom and top positions of the partition, is defined by eight fixed points, while the partition wall is decentralized to seven pairs of control points to keep the thickness of the

Table 1. Location of shape control points of internal partition.

Parameters	Position (Original)	Position (After 10 generation)	Position (After (After 15 generation)	Position (After 20 generation)
Point Pair 1	(0.5, 0.0)	(0.500, 0.0)	(0.500, 0.0)	(0.500, 0.0)
Point Pair 2	(0.5, 0.1)	(0.431, 0.1)	(0.527, 0.1)	(0.527, 0.1)
Point Pair 3	(0.5, 0.2)	(0.580, 0.2)	(0.441, 0.2)	(0.505, 0.2)
Point Pair 4	(0.5, 0.3)	(0.580, 0.3)	(0.548, 0.3)	(0.452, 0.3)
Point Pair 5	(0.5, 0.4)	(0.431, 0.4)	(0.567, 0.4)	(0.569, 0.4)
Point Pair 6	(0.5, 0.5)	(0.441, 0.5)	(0.431, 0.5)	(0.559, 0.5)
Point Pair 7	(0.5, 0.6)	(0.559, 0.6)	(0.537, 0.6)	(0.559, 0.6)
Point Pair 8	(0.5, 0.7)	(0.431, 0.7)	(0.431, 0.7)	(0.431, 0.7)
Point Pair 9	(0.5, 0.8)	(0.500, 0.8)	(0.500, 0.8)	(0.500, 0.8)

partition constant. These control points are to be moved in the shape optimization procedure as described in Fig. 3. The initial locations of the control point pairs are given by the second column in Table 1. The locations are marked by the positions of control points over the left-hand side of the partition wall (Fig. 14). The wall thickness is fixed as 0.02 m.

The control parameters of MIGA based on iSight platform are tabulated in Table 2. The convergence criteria used is to ensure that the values for the objective function between the two consecutive iterations is lower than 10^{-2}.

Using the multi-island GA, the shape of the partition is varied and optimized. Starting from the initial configuration shown in Fig. 17(a), the evolution of the partition shape is illustrated by Fig. 17(b) (after 10 generation) and Fig. 17(c) (after 15 generation), before reaching the final configuration shown in Fig. 17(d). Evolution of the control points during the optimization procedure is given by Table 1.

It can be seen from Fig. 17 that convergence can be achieved relatively quickly using the present optimization strategy. More specifically, the SPL inside the box varies from 106 dB to 116 dB in the initial configuration. After 10 generations, the variation range retreats to 104 dB–114 dB. Continuing its evolution, the optimal configuration is reached in Fig. 17(d), in which the SPL inside the box varies from 95 dB to 109 dB. As compared to the initial straight partition, the optimized partition shape reduces the average SPL inside the box from 111 dB to 100 dB, corresponding to a reduction of 11 dB in the targeted area.

Table 2. MIGA parameters.

Parameters	Value
Sub-population size	25
Number of island	10
Number of generation	20
Rate of crossover	0.8
Rate of mutation	0.01
Rate of migration	0.5
Interval of migration	3
Total iterative number	5000

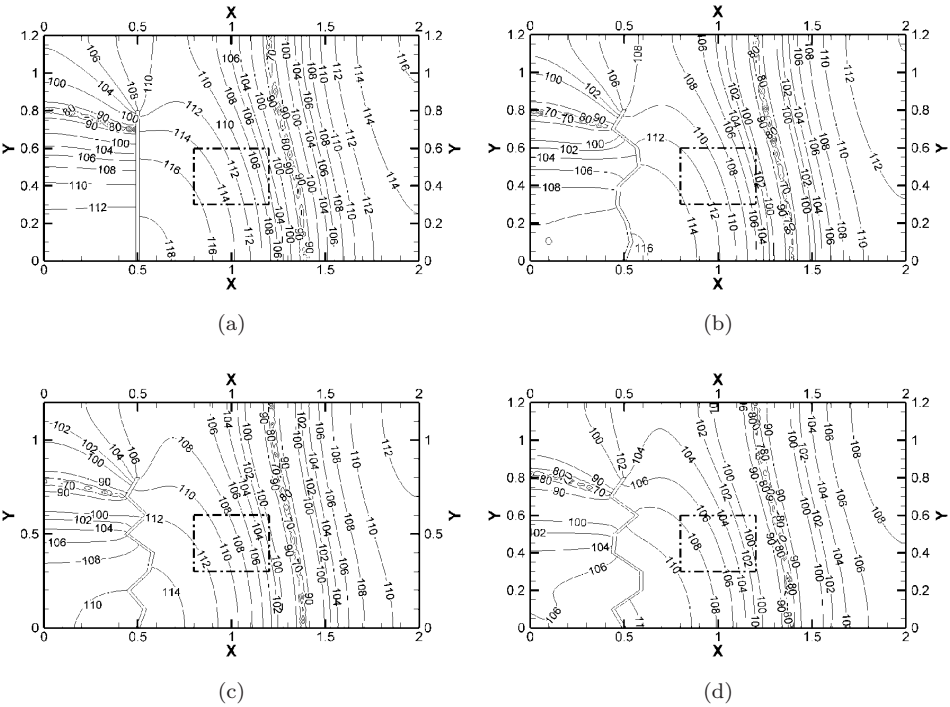

Fig. 17. Sound pressure distribution inside the enclosure with an internal partial partition. (a) Straight partition before optimization, (b) after 10 generations, (c) after 15 generations and (d) after 20 generations, average SPL level reduced from 111 dB to 100 dB, as compared to the initial configuration.

Results also suggest that the acoustic field distribution inside the enclosure, especially within the predefined area, can be significantly altered by appropriate changes in its geometry or internal geometrical setting. This can be interpreted as a result of the alteration to the mode-shapes of the enclosure. This is particularly relevant in some applications in which noise control inside the entire volume is difficult to achieve. Creation of a quite zone within a limited area may be an attractive and feasible solution. The presently proposed methodology may find its applications in those cases.

4. Conclusions

A general procedure is proposed to deal with the general problem of internal sound field prediction and the optimization of the boundary shape. Owing to the compactly supported orthogonal property of the wavelet and its extraordinary fitting capability, Daubechies wavelet scaling function is proposed as a global basis function to expand the unknown sound pressure under the general Galerkin framework. A method named vertex-driven shape optimization is established and demonstrated.

Using acoustically rigid rectangular cavity as a benchmark problem, the proposed WGM is shown to be able to achieve high accuracy without any boundary meshing. The accuracy of the WGM strongly depends on the resolution level m and the number of Gauss integration points, and in principle also on the wavelet support length L, but to a much less extent. As long as the support length $L$is larger than the expansion domain, the accuracy keeps almost the same. The accuracy increases when the value of the resolution level m increases to a certain value, beyond which ill-conditioned problem may take place. This ill-condition problem can be eased by increasing the number of Gauss integration points based on the adaptive refining strategy proposed in the paper.

Based on the strong ability of wavelet scale functions in approximating unknown functions in a relative large interval, the proposed WGM allows global expansion and therefore allows flexible handling of the cavity boundaries in a unified way without meshing the geometry model like FEM/BEM usually does. This empowers the new approach with its superiority in acoustic mutation and shape optimization problems over other conventional simulation methods. Potentials of the approach are demonstrated using a polygonal cavity with internal partial partition by following a vertex-driven shape optimization procedure proposed in this paper.

As a final note, it is relevant to mention that, although numerical studies reported in this paper only focused on two-dimensional polygonal cavities, in principle, the proposed methodology should apply to more complex cavities in which the boundary segments can be described by curved segments of any shapes such as arcs or spline, as long as they can be described by relatively simple curve functions. It is also possible to extend the method to three-dimensional problems.

Acknowledgments

The authors wish to acknowledge a grant from Research Grants Council of Hong Kong Special Administrative Region, China (PolyU 152026/14E).

References

Anyunzoghe, E. and Cheng, L. [2002] "Improved integro-modal approach with pressure distribution assessment and the use of overlapped cavities," *Applied Acoustics* **63**(11), 1233–1255.

Bai, M. R. [1992] "Study of acoustic resonance in enclosures using eigenanalysis based on boundary element methods," *The Journal of the Acoustical Society of America* **91**(5), 2529–2538.

Chen, M. Q., Hwang, C. and Shih, Y. P. [1996] "The computation of wavelet-galerkin approximation on a bounded interval," *International Journal for Numerical Methods in Engineering* **39**(17), 2921–2944.

Chen, L. M., Chen, M. J., Pei, Y. M., Zhang, Y. H. and Fang, D. N. [2012] "Optimal design of sandwich beams with lightweight cores in three-point bending," *International Journal of Applied Mechanics* **4**(03).

Chiu, M. C. and Chang, Y. C. [2008] "Shape optimization of multi-chamber cross-flow mufflers by SA optimization," *Journal of Sound and Vibration* **312**(3), 526–550.

Dowell, E. H., Gorman III, G. and Smith, D. A. [1977] "Acoustoelasticity: General theory, acoustic natural modes and forced response to sinusoidal excitation, including comparisons with experiment," *Journal of Sound and Vibration* **52**(4), 519–542.

Fahy, F. J. and Gardonio, P. [2007] *Sound and Structural Vibration*: *Radiation*, *Transmission and Response* (Academic Press, New York).

Geng, Q. and Li, Y. [2012] "Analysis of dynamic and acoustic radiation characters for a flat plate under thermal environments," *International Journal of Applied Mechanics* **4**(03).

Givoli, D. and Demchenko, T. [2000] "A boundary-perturbation finite element approach for shape optimization," *International Journal for Numerical Methods in Engineering* **47**(4), 801–819.

Jaffard, S. [1992] "Wavelet methods for fast resolution of elliptic problems," *SIAM Journal on Numerical Analysis* **29**(4), 965–986.

Koo, B. U., Ih, J. G. and Lee, B. C. [1998] "Acoustic shape sensitivity analysis using the boundary integral equation," *The Journal of the Acoustical Society of America* **104**(5), 2851–2860.

Kost, B., Baumann, B., Germer, M., Wolff, M. and Rosenkranz, M. [2011] "Numerical shape optimization of photoacoustic resonators," *Applied Physics B* **102**(1), 87–93.

Lee, J. W. and Kim, Y. Y. [2009] "Topology optimization of muffler internal partitions for improving acoustical attenuation performance," *International Journal for Numerical Methods in Engineering* **80**(4), 455–477.

Levine, H. [2001] "Acoustical cavity excitation," *The Journal of the Acoustical Society of America* **109**(6), 2555–2565.

Liu, Z. S., Lu, C., Wang, Y. Y., Lee, H. P., Koh, Y. K. and Lee, K. S. [2006a] "Prediction of noise inside tracked vehicles," *Applied Acoustics* **67**(1), 74–91.

Liu, Z. S., Lee, H. P. and Lu, C. [2006b] "Passive and active interior noise control of box structures using the structural intensity method," *Applied Acoustics* **67**(2), 112–134.

Maleknejad, K. and Lotfi, T. [2006] "Expansion method for linear integral equations by cardinal B-spline wavelet and Shannon wavelet as bases for obtain Galerkin system," *Applied Mathematics and Computation* **175**(1), 347–355.

Marburg, S. [2002] "Efficient optimization of a noise transfer function by modification of a shell structure geometry — Part I: Theory," *Structural and Multidisciplinary Optimization* **24**(1), 51–59.

Marburg, S. and Hardtke, H. J. [2001] "Shape optimization of a vehicle hat-shelf: Improving acoustic properties for different load cases by maximizing first eigenfrequency," *Computers & Structures* **79**(20), 1943–1957.

Marburg, S. and Hardtke, H. J. [2002] "A general concept for design modification of shell meshes in structural-acoustic optimization — Part II: Application to a floor panel in sedan interior noise problems," *Finite Elements in Analysis and Design* **38**(8), 737–754.

Mimani, A. and Munjal, M. L. [2011] 3D acoustic analysis of spherical chamber having single inlet and multiple outlet: An impedance matrix approach, *International Journal of Applied Mechanics* **3**(04), 685–710.

Missaoui, J. and Cheng, L. [1997] "A combined integro-modal approach for predicting acoustic properties of irregular-shaped cavities," *The Journal of the Acoustical Society of America* **101**(6), 3313–3321.

Peng, S. Z. and Cheng, L. [2008] "An improved acoustical wave propagator method and its application to a duct structure," *The Journal of the Acoustical Society of America* **123**(2), 610–621.

Renner, G. and Ekárt, A. [2003] "Genetic algorithms in computer aided design," *Computer-Aided Design* **35**(8), 709–726.

Succi, G. P. [1987] "The interior acoustic field of an automobile cabin," *The Journal of the Acoustical Society of America* **81**(6), 1688–1694.

Wang, G. [1998] "Analysis of electromagnetic scattering from conducting bodies of revolution using orthogonal wavelet expansions," *Electromagnetic Compatibility, IEEE Transactions on* **40**(1), 1–11.

Zheng, H. and Wei, Z. [2013] "Vibroacoustic analysis of stiffened plates with nonuniform boundary conditions," *International Journal of Applied Mechanics* **5**(04).